Chapter 5: Neutral Density Profile

The question of what the neutral density profile is for Argon within the Helimak will try to be addressed theoretically here.

5.1 Motivation

Ionization rate data is available from the Bogaerts[4] CR model used in calculating density and temperature, but another source of Argon ionization rates is referenced from Arnaud et al[12]. The velocity integrated cross section $\langle \sigma_{ion} v \rangle$ is plotted in figure 5.1 from both sources for neutral Argon, as well as the first two ionization states.

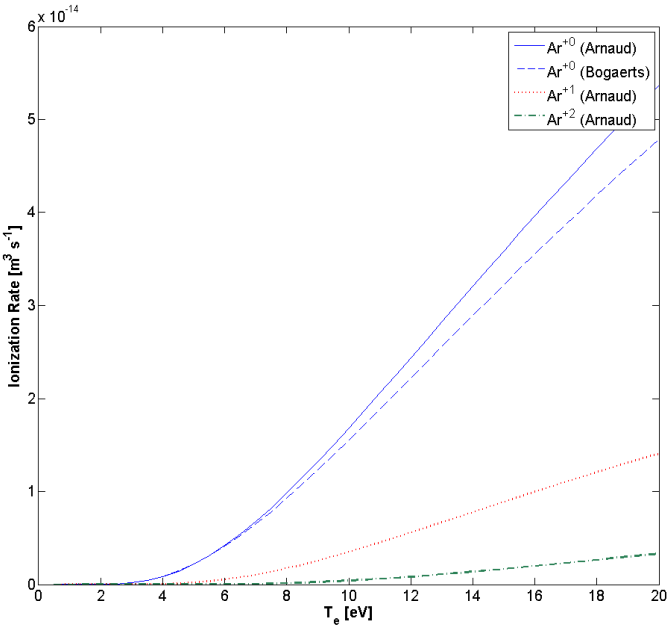

Figure 5.1: Ionization rates for Argon from Bogaerts[4] and Arnaud[12].

The ionization rate for neutral Argon at $T_e = 10eV$ and $n_e = 5E16\ m^{-3}$ is about $K_{ion} = n_e \langle \sigma_{ion} v \rangle = 800\ s^{-1}$. Using $v_{th} = 340\ \frac{m}{s}$ (T=300K) gives a mean free path of an atom before being ionized of $\lambda_{ion} = \frac{v_{th}}{K_{ion}} = 0.4\ m$. The Helimak's scale is of 1m, which

implies that a significant fraction of the neutral atoms could be ionized while traversing the Helimak chamber. That is, it would be hard to justify that the profile must be flat.

The ionization rate would be a peaked profile since the electron density and temperature also have peaked profiles. Also, since the neutral atoms velocities should be close to thermal distribution, the mean free path would depend on exactly what velocity each atom is traveling. To find the actual profile of the neutral density, the non-local and thermal effects should be included.

The neutral-neutral collisional mean free path as defined by $\lambda_{00} = \frac{1}{n_0 \sigma_{00}} \cong 10m$, with $\sigma_{00} = 36\ \text{Å}^2$ for Argon [ref. ??], which is larger than the dimension of the Helimak chamber. The gas is in the molecular flow, or ballistic, regime where collisions with the walls are more frequent than with other atoms.

5.2 KINETIC MODEL

A kinetic model is used to solve for the neutral density. Even though this approach is computationally intensive, it is straightforward. The evolution of the gas can be described by the Boltzmann equation, (5.1), which models the distribution of particles in velocity and spatial dimensions $f(\overline{x}, \overline{v}, t)$. For three spatial dimensions, the distribution function has six dimensions plus time.

$$\frac{\partial f}{\partial t} + \overline{\nabla}_x \cdot (\mathrm{f}\,\overline{v}) + \overline{\nabla}_v \cdot (\mathrm{f}\,\overline{a}) = \frac{\partial f}{\partial t}_{coll} + s \qquad (5.1)$$

The first term on the left hand side, $\frac{\partial f}{\partial t}$, is simply the time rate of change of the distribution at a particular velocity, position, and time. The second term, $\overline{\nabla}_x \cdot (\mathrm{f}\,\overline{v})$, represents the streaming of particles through space. The third term, $\overline{\nabla}_v \cdot (\mathrm{f}\,\overline{a})$, represents how forces move the particles through velocity space. The acceleration vector can also be a function of both position and velocity $\overline{a}(\overline{x}, \overline{v}, t)$. The first term on the RHS, $\frac{\partial f}{\partial t}_{coll}$, is the effect of collisions between particles in the distribution as well as other species of particles, and also moves particles around in velocity space. This term can be complicated and would in reality be a functional of the distribution itself. The last term, $s(\overline{x}, \overline{v}, t)$, is the source term which can add or remove particles, such as through ionization and recombination.

A neutral gas does not produce nor interact with electromagnetic fields. The interaction with the gravitational force can also be neglected since $\frac{3}{2}kT \gg mgh$. This allows the dropping of the external forces altogether. Since the neutral collision rate is very low, the collision term will also be dropped. Since a steady state solution is desired this leaves eq. 5.2. The source term within the plasma will only be due to ionization. Recombination is much slower within the plasma by over an order of magnitude and so will be dropped. This leaves $s = -f\,K(n_e, T_e)$. The source term will need to include recombination at the wall somewhere, but will be dealt with separately.

$$\overline{\nabla}_x \cdot (\mathrm{f}\,\overline{v}) = -f\,K(n_e, T_e) \tag{5.2}$$

If a particular direction is chosen, $v\frac{\partial}{\partial l} \equiv \bar{v} \cdot \overline{\nabla}_x$, then the equation can be re-arranged into eq. 5.3. The ionization rate can also be written as a function of position since the electron density and temperature are functions of position. This equation can be directly integrated in the form of eq. 5.4 if the position is also parameterized in terms of l to give eq. 5.5, where $L(r, z, \hat{r} \cdot \hat{v}, \hat{z} \cdot \hat{v})$ is the distance to the wall from the test position along the direction $-\hat{v}$.

$$v\frac{\partial f}{\partial l} = -fK(\bar{x}) \tag{5.3}$$

$$\frac{1}{f}df = -\frac{1}{v}K\left(\overline{x'}(l)\right)dl \tag{5.4}$$

$$f(\bar{x}, \bar{v}) = f(\bar{x}_0, \bar{v}) \exp\left[-\frac{1}{v}\int_0^L dl\, K(\bar{x}_0 + l\hat{v})\right] \tag{5.5}$$

The position the path intersects the wall is $\bar{x}_0 \equiv \bar{x} - L\hat{v}$. The electron density and temperature are assumed to be cylindrically symmetric, so the rate K should only depend on the radial coordinate. The radius can be parameterized in terms of l to give eq. 5.6. Using spherical coordinates for the velocity, and $\hat{r} \cdot \hat{v} \equiv \sin\varphi\cos\theta$ and $\hat{z} \cdot \hat{v} \equiv \cos\varphi$ at the point where the solution is being computed.

$$r' = [(r + (l - L)\sin\varphi\cos\theta)^2 + (l - L)^2\sin^2\varphi\cos^2\theta]^{1/2} \tag{5.6}$$

The next task is to define the function L, which depends on the geometry of the Helimak. The path can be broken into two components, one perpendicular to the z-axis and one parallel. If the floor and ceiling of the Helimak are ignored for a moment, the perpendicular component has only two possible cases. One where the path originates

from the outer wall, and one from the inner wall, depending on the value of θ, which are depicted in figure 5.2.

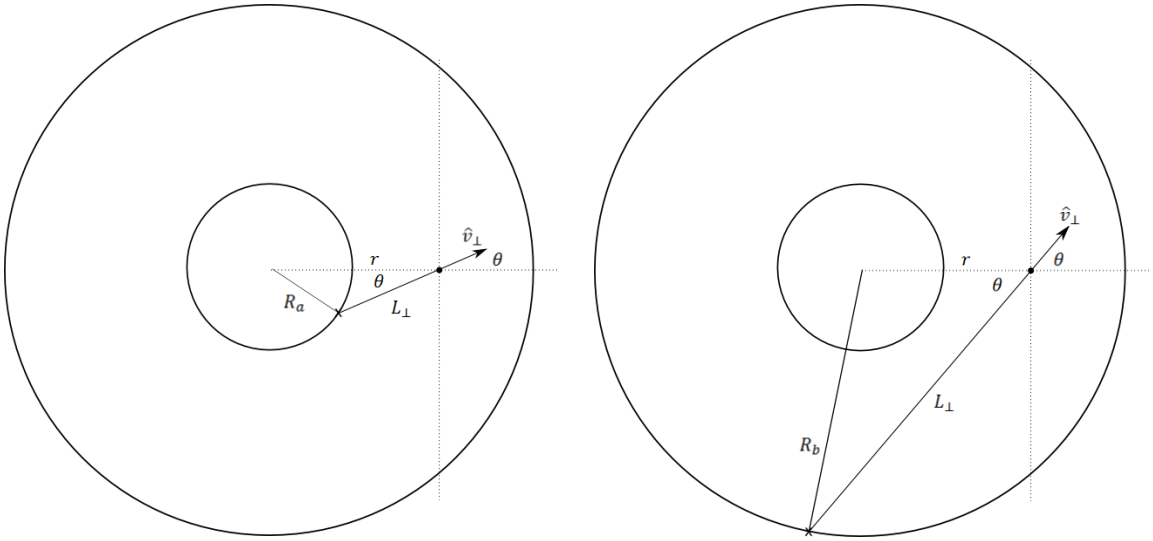

Figure 5.2: Component of path perpendicular to z-axis of Helimak. Can intersect either inner wall or outer wall depending on θ. (a) [left] Path Intersects Inner Wall. (b) [right] Path Intersects Outer Wall.

The law of cosines can be used to derive the expressions for $L_\perp$. For the inner wall this gives $R_a^2 = r^2 + L_\perp^2 - 2rL_\perp \cos\theta$, and for the outer wall $R_b^2 = r^2 + L_\perp^2 - 2rL_\perp \cos\theta$, which can be solved using the quadratic formula. At the transition point the path is tangent to the inner wall giving $\sin\theta_t = \frac{R_a}{r}$. When $\theta \leq \theta_t$ the inner wall value is used, and when $\theta > \theta_t$ the outer wall is used giving eq. 5.7.

$$L_\perp = r\cos\theta + \begin{cases} -\sqrt{R_a^2 - r^2\sin^2\theta}\,, & \theta \leq \theta_t \\ \sqrt{R_b^2 - r^2\sin^2\theta}\,, & \theta > \theta_t \end{cases} \tag{5.7}$$

The parallel component is simply the distance to either the floor or the ceiling. However, there are additional restrictions now to match both the wall and the floor and ceiling conditions depending on φ depicted in figure 5.3. The solution is summarized in eq. 5.9.

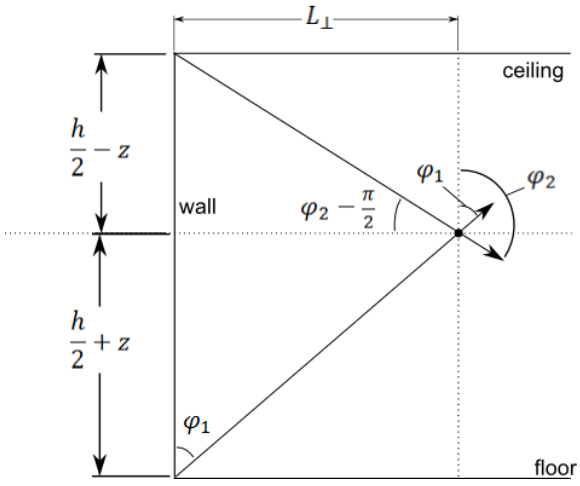

Figure 5.3: Matching wall condition with floor and ceiling.

$$\varphi_1 = \tan^{-1}\left(\frac{L_\perp}{\left(\frac{h}{2}+z\right)}\right)$$
$$\varphi_2 = \tan^{-1}\left(\frac{\left(\frac{h}{2}-z\right)}{L_\perp}\right) + \frac{\pi}{2} \tag{5.8}$$

$$L = \begin{cases} \left(\frac{h}{2}+z\right)\sec\varphi\,, & 0 \le \varphi \le \varphi_1 \\ L_\perp \csc\varphi\,, & \varphi_1 < \varphi < \varphi_2 \\ \left(\frac{h}{2}-z\right)(-\sec\varphi), & \varphi_2 \le \varphi \le \pi \end{cases} \tag{5.9}$$

The solution in eq. 5.5 still depends on the value of the distribution at the boundary $f(\bar{x}_0, \bar{v})$. The boundary condition is that the total flux at the walls, minus the source, must be zero. The total particle flux is the first velocity moment of the

distribution. For velocities going into the wall, the distribution is found using eq. 5.5, where $f(\bar{x}_0, \bar{v})$ is the value at some other wall coming inward. The distribution coming from the wall must be found to match the boundary condition.

To simplify the process of solving the boundary condition, it will be assumed that the part of the distribution not determined by 5.5 is Maxwellian in shape. The justification for this is that particles will scatter off the walls changing their direction and energy, and would eventually come into thermal equilibrium with the walls anyway after scattering many times.

The distribution is divided into two components with n^- and $\bar{\Gamma}^-$ defined as the particle density and flux from the part of the distribution from 5.5 going into the wall, and n^+ and $\bar{\Gamma}^+$ from the rest of the distribution that is Maxwellian like. The total density and flux at the wall is then $n = n^- + n^+$ and $\bar{\Gamma} = \bar{\Gamma}^- + \bar{\Gamma}^+$. For the walls the condition is $\hat{q} \cdot \bar{\Gamma} = 0$, where $\hat{q}$ is the inward directed normal vector of the wall surface. The corners between the floor or ceiling and the inner or outer wall must satisfy both surface conditions.

For the flat surfaces, $\hat{q} \cdot \bar{\Gamma}^+$ is found by integrating over the half Maxwellian distribution, and results in eq. 5.11. The corners are trickier because in order to satisfy two conditions simultaneously, the distribution must have two free parameters. In the corner $\bar{\Gamma}^-$ is only defined for one quarter of the directions, so the other three quarter directions are Maxwellian like, but cannot be isotropic. If n^+ is defined in the corner as in

eq 5.10, and assuming that $\hat{q}_1 \cdot \hat{q}_2 = 0$, then the positive flux in the two directions is found from eq. 5.12 and 5.13. $v_{th} = \sqrt{\frac{2\,kT}{m}}$.

$$n^+ = \begin{cases} n_2^+, & \hat{q}_1 \cdot \hat{v} < 0, \hat{q}_2 \cdot \hat{v} > 0 \\ n_1^+ \epsilon_1 + n_2^+ \epsilon_2, & \hat{q}_1 \cdot \hat{v} > 0, \hat{q}_2 \cdot \hat{v} > 0 \\ n_1^+, & \hat{q}_1 \cdot \hat{v} > 0, \hat{q}_2 \cdot \hat{v} < 0 \end{cases} \tag{5.10}$$

where $\epsilon_1 = \frac{(\hat{q}_1 \cdot \hat{v})^2}{(\hat{q}_1 \cdot \hat{v})^2 + (\hat{q}_2 \cdot \hat{v})^2}$, and $\epsilon_2 = \frac{(\hat{q}_2 \cdot \hat{v})^2}{(\hat{q}_1 \cdot \hat{v})^2 + (\hat{q}_2 \cdot \hat{v})^2}$

$$\hat{q} \cdot \bar{\Gamma}^+ = \frac{v_{th}}{\sqrt{\pi}} n^+ \tag{5.11}$$

$$\hat{q}_1 \cdot \bar{\Gamma}^+ = \frac{v_{th}}{6\sqrt{\pi}} (5n_1^+ - 2n_2^+) \tag{5.12}$$

$$\hat{q}_2 \cdot \bar{\Gamma}^+ = \frac{v_{th}}{6\sqrt{\pi}} (5n_2^+ - 2n_1^+) \tag{5.13}$$

$$\hat{q} \cdot \bar{\Gamma}^- = \int_{\hat{q} \cdot \bar{v} < 0} d\bar{v} (\hat{q} \cdot \bar{v}) f(\bar{x}, \bar{v}) \tag{5.14}$$

The boundary is then discretized, and coefficients computed to give the contribution of each boundary element to the outward particle flux at every other boundary element using eq. 5.5, and eq. 5.14. The outward flux at each point is then found by summing over all of the contributions as in eq. 5.15 for flat surfaces, and 5.16 for the corners. The addition of s_j is the source term from recombination of ions at the wall. The inward directed density at the wall can then found by solving 5.15 and 5.16 by iteration.

$$\hat{q}_i \cdot \bar{\Gamma}_i^- = \sum_{j \neq i} A_{ij}\left[n_j^+ + s_j\right] = \hat{q}_i \cdot \bar{\Gamma}_i^+ = \frac{v_{th}}{\sqrt{\pi}} n_i^+ \tag{5.15}$$

$$\sum_{j \neq i} A_{ij}\left[n_j^+ + s_j\right] = \frac{v_{th}}{6\sqrt{\pi}}(5n_i^+ - 2n_k^+) \tag{5.16}$$

Assuming a Maxwellian distribution at the boundary has another important feature. Since the inward half of the distribution can then be written as eq. 5.17, integrating 5.5 over all velocity space to get the first two moments of the distribution can be simplified by expressing the integral over the magnitude of velocity as a pre-computed function. The integral in the exponent of 5.5 can be defined as $v_K = \int_0^L dl\, K(\bar{x}_0 + l\hat{v})$, a characteristic velocity below which the distribution is highly attenuated. Using the dimensionless parameters $\alpha = v_K/v_{th}$ and $\beta = v/v_{th}$, the first two moments can be written as eq. 5.18 and 5.19.

$$f(\bar{x}_0, \bar{v}) = n^+(\bar{x}_0) 2\left(\sqrt{\pi} v_{th}\right)^{-3} \exp[-v^2/v_{th}^2] \tag{5.17}$$

$$n(\bar{x}) = \frac{2}{\pi^{3/2}} \iint d\theta d\varphi \sin\varphi\, n^+(\bar{x}_0) M(\alpha) \tag{5.18}$$

$$\bar{\Gamma}(\bar{x}) = \frac{2v_{th}}{\pi^{3/2}} \iint d\theta d\varphi \sin\varphi\, \hat{v} n^+(\bar{x}_0) N(\alpha) \tag{5.19}$$

$$M(\alpha) = \int_0^\infty d\beta \beta^2 \exp[-\beta^2 - \alpha/\beta] \tag{5.20}$$

$$N(\alpha) = \int_0^\infty d\beta \beta^3 \exp[-\beta^2 - \alpha/\beta] \tag{5.21}$$

The two functions $M(\alpha)$ and $N(\alpha)$, plotted in figure 5.4, can be pre-computed and placed in a lookup table. The integral's over θ and φ must still be calculated at every location since $\bar{x}_0$ and α are complicated functions of θ, φ, r and z.

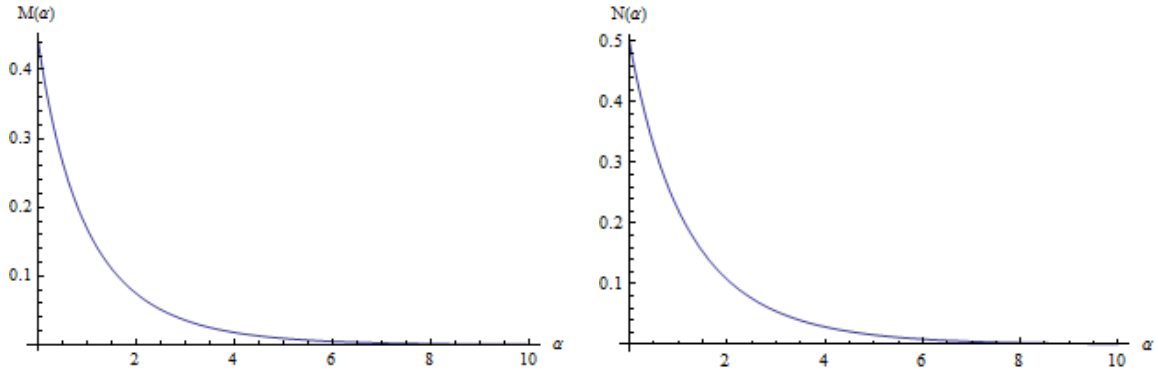

Figure 5.4: Integrals $M(\alpha)$ and $N(\alpha)$ plotted over a range of the parameter.

There are several obvious symmetries that will be used to minimize the amount of computation required. The solution will be axially symmetric, so it needs only be calculated for r and z. There is an up-down symmetry so that only the +z positions need to be computed. There is also reflection symmetry in velocity space along the azimuthal direction of the Helimak, so only half of the directions need to be computed.

The integral over θ and φ must be computed numerically for a discrete set of points on the unit sphere. If the points are placed at evenly spaced increments of θ and φ, as depicted in figure 5.5, then bilinear interpolation (eq 5.22) can be used between the points.

$$f_{ij}(\theta,\varphi) = \frac{1}{\Delta\theta\Delta\varphi}\big[f(\theta_i,\varphi_j)(\theta_{i+1}-\theta)(\varphi_{j+1}-\varphi) + f(\theta_{i+1},\varphi_j)(\theta-\theta_i)(\varphi_{j+1}-\varphi) + f(\theta_i,\varphi_{j+1})(\theta_{i+1}-\theta)(\varphi-\varphi_j) + f(\theta_{i+1},\varphi_{j+1})(\theta-\theta_i)(\varphi-\varphi_j)\big] \tag{5.22}$$

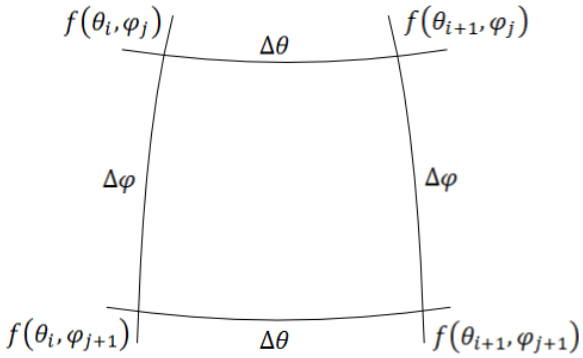

Figure 5.5: Discrete segment on the unit sphere.

The interpolated function can be integrated over its domain analytically (eq. 5.23). All of the discrete integrals can be summed to give the total integral over the sphere. The total integral simplifies to eq. 5.24.

$$\begin{aligned} I_{ij} &= \int_{\theta_i}^{\theta_{i+1}} d\theta \int_{\varphi_j}^{\varphi_{j+1}} d\varphi \sin\varphi\, f_{ij}(\theta,\varphi) \\ &= \frac{1}{2}\Delta\theta\Bigg[\Big(f(\theta_i,\varphi_j)+f(\theta_{i+1},\varphi_j)\Big)\Bigg[\cos\varphi_j - \frac{\sin\varphi_{j+1}-\sin\varphi_j}{\Delta\varphi}\Bigg] \\ &\quad - \Big(f(\theta_i,\varphi_{j+1})+f(\theta_{i+1},\varphi_{j+1})\Big)\Bigg[\cos\varphi_{j+1} - \frac{\sin\varphi_{j+1}-\sin\varphi_j}{\Delta\varphi}\Bigg]\Bigg] \end{aligned} \tag{5.23}$$

$$I = 2\pi\left(1 - \frac{\sin\Delta\varphi}{\Delta\varphi}\right)[f(\varphi = 0) + f(\varphi = \pi)] + 2\frac{\Delta\theta}{\Delta\varphi}(1 - \cos\Delta\varphi)\sum_{j=2}^{\frac{\pi}{\Delta\varphi}}\sum_{i=1}^{\frac{2\pi}{\Delta\theta}}\sin\varphi_j\, f(\theta_i, \varphi_j) \quad (5.24)$$

For the numerical runs, a radial profile for electron density and temperature are needed to define the ionization rate function K in eq. 5.5. Also needed is the recombination source profile on the walls. For n_e and T_e, a fitting function is used to approximate their profile based on probe data. The function used is eq. 5.25, where A is the maximum value of either n_e or T_e, γ is the ratio of the value at the outer wall to the maximum value, $x = \frac{r-R_a}{R_b-R_a}$, $x_p = \frac{r_p-R_a}{R_b-R_a}$ (where r_p is the location of the profile peak), and $y = \left(\frac{0.5-x_p}{x_p^2-x_p}\right)x^2 + \left(1 - \left(\frac{0.5-x_p}{x_p^2-x_p}\right)\right)x$. A value of $\gamma = 0.5$ and $r_p = 1.1m$ was used for n_e, and $\gamma = 0.4$ and $r_p = 1m$ for T_e. An example fit is shown in figure 5.6.

$$h(x) = A\left(\frac{\gamma}{2}(1 - \cos(\pi y(x))) + \left(1 - \frac{\gamma}{2}\right)\sin^3(\pi y(x))\right) \quad (5.25)$$

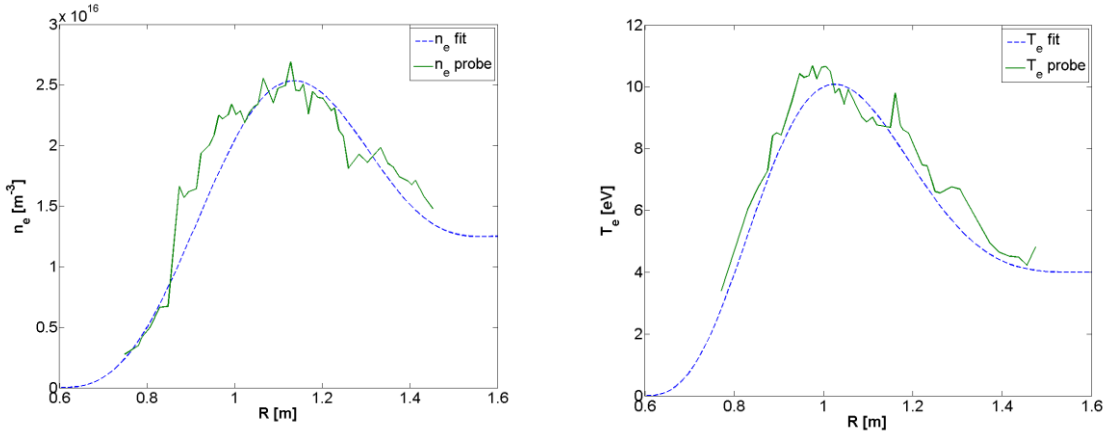

Figure 5.6: Fitting function for n_e or T_e profiles.

The recombination profile is a bit trickier to know. Ions should mostly flow vertically along field lines, which means that recombination will occur at the ceiling and floor, and not on the inner and outer walls. It will be assumed that the recombination rate is proportional to the sound speed, the electron density, and the radius: $\Gamma_{recomb} \propto C_s n_e R \propto T_e^{1/2} n_e R$. This is because the ion velocity along the field lines should scale with the sound speed, and the ion density should scale with the electron density. The pitch of the field lines also changes with radius due to the 1/R scaling of the toroidal field. So the vertical component of the ion velocity should scale with R. However, this only gives a shape of the recombination profile, but not the magnitude. Given a fixed ionization rate profile, the neutral density at any point should be proportional to the recombination rate at the wall. Once the solution is computed using some arbitrary magnitude for the recombination rate, the whole solution can be re-scaled so that the average neutral density matches the measured value in eq. 4.7. Since the initial scale of the solution is then completely arbitrary, only the shape of the solution matters, it only needs to be computed in normalized units.

5.3 Solution Profiles

For an example solution, the plasma parameters used are peak values for $T_e = 10eV$ and $n_e = 5E16\ m^{-3}$, and the fitting functions. The peak n_e used is higher than seen in probe data and are taken from the example calculation in chapter 4 using spectroscopic measurements.

The neutral density is plotted in figure 5.7a, which is only the upper half of the chamber, and has been normalized to the average density. The solution shows variation in the density in both r and z. The spectroscopic measurements are a chord integral through the z-direction, and so what is important is the average density along each vertical chord, which is plotted in fig 5.7b. A profile like this could be used now to make the next correction to the spectroscopically measured values of n_e and T_e in chapter 4.

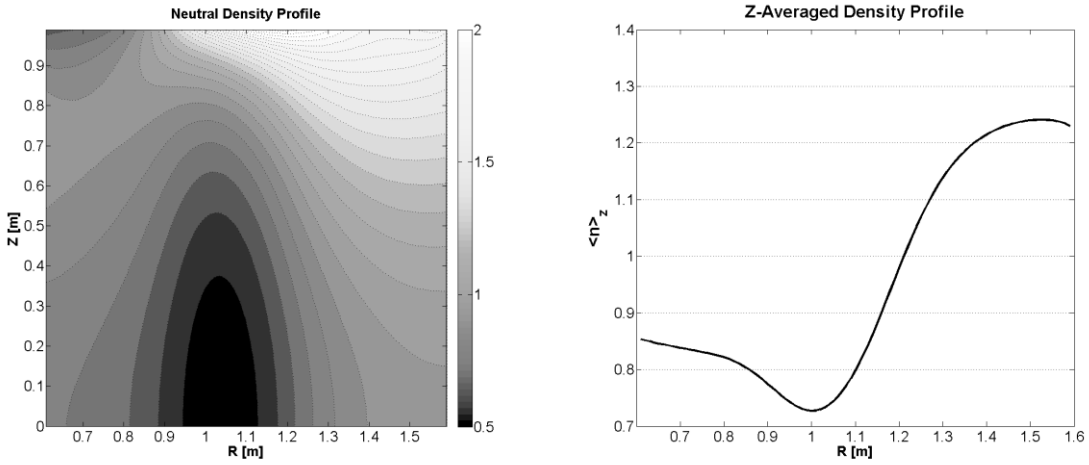

Figure 5.7 The first moment of $f(\bar{x}, \bar{v})$ plotted in upper half of Helimak chamber. (a) [left] $n(\bar{x})$, normalized to average density. (b) [right] z-average of normalized $n(\bar{x})$.

Also plotted in figure 5.8a is a streamline plot of the neutral flux density, which is the second moment of the distribution. The neutrals originate at the top and bottom from recombination, and on average flow into the region of highest ionization. This is only an average process since the individual atoms are simply bouncing from wall to wall until they are ionized. The peak averaged speed of the neutrals is around 150m/s near the top and bottom.

Since the neutral flux density and the ion flux density must match at the boundary, this could also indicate the magnitude of the ion velocity near the top and bottom that would be needed to be self-consistent. The ratio $\frac{n_{ArI}}{n_{ArII}} \approx 12$ in this location, which means the ions would need a vertical average velocity of about 1800m/s to balance the particle flux. This is a significant fraction of the ion sound speed $C_s = \sqrt{\frac{kT_e}{m_{Ar}}}$, which at 10eV is about 4900m/s.

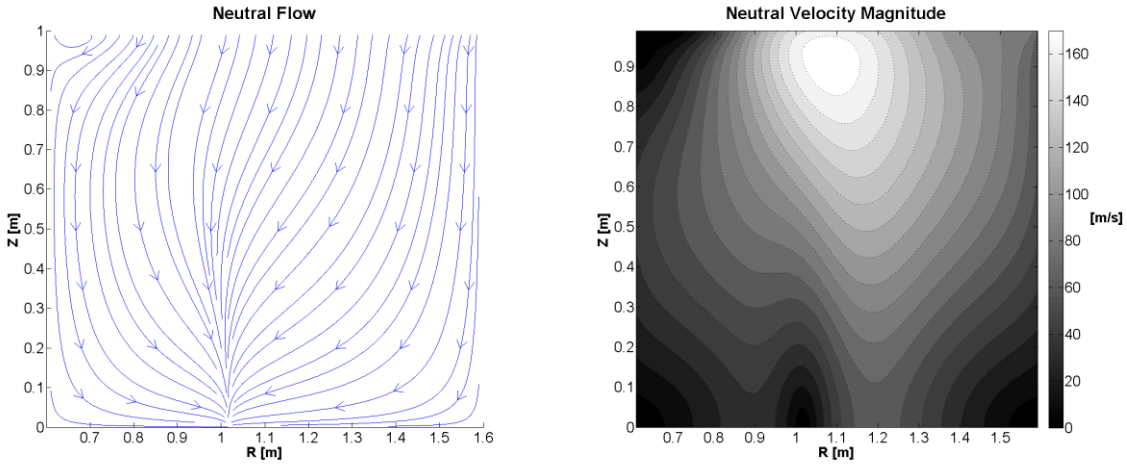

Figure 5.8 The second moment of $f(\bar{x}, \bar{v})$ in the upper half of chamber. (a) [left] streamlines of flux density $\bar{\Gamma}(\bar{x})$. (b) [right] magnitude of $v = |\bar{\Gamma}(\bar{x}) / n(\bar{x})|$.